


Reversible optical control of F_1F_o -ATP synthase using photoswitchable inhibitors

Bianca Eisel^{1,2,*}, Felix W.W. Hartrampf^{3,*}, Thomas Meier^{1,2}  and Dirk Trauner^{3,4} 

1 Department of Structural Biology, Max Planck Institute of Biophysics, Frankfurt am Main, Germany

2 Department of Life Sciences, Imperial College London, UK

3 Department of Chemistry, University of Munich, Germany

4 Department of Chemistry, New York University, NY, USA

Correspondence

T. Meier, Department of Life Sciences,
Imperial College London, Exhibition Road,
London SW7 2AZ, UK
Tel: +44 2075943056
E-mail: t.meier@imperial.ac.uk
and

D. Trauner, Department of Chemistry, New
York University, 100 Washington Square
East, New York, USA
Tel: +1 2129983747
E-mail: dirktrauner@nyu.edu

F_1F_o -ATP synthase is one of the best studied macromolecular machines in nature. It can be inhibited by a range of small molecules, which include the polyphenols, resveratrol and piceatannol. Here, we introduce Photoswitchable Inhibitors of ATP Synthase, termed PIAS, which were synthetically derived from these polyphenols. They can be used to reversibly control the enzymatic activity of purified yeast *Yarrowia lipolytica* ATP synthase by light. Our experiments indicate that the PIAS bind to the same site in the ATP synthase F_1 complex as the polyphenols in their *trans* form, but they do not bind in their *cis* form. The PIAS could be useful tools for the optical precision control of ATP synthase in a variety of biochemical and biotechnological applications.

Keywords: photopharmacology; *Yarrowia lipolytica* F_1F_o -ATP synthase

*Contributed equally to this work.

(Received 1 November 2017, revised 13
December 2017, accepted 22 December
2017, available online 1 February 2018)

doi:10.1002/1873-3468.12958

Edited by Peter Brzezinski

F_1F_o -type ATP synthase is a membrane-embedded, macromolecular rotary machine that discharges the transmembrane electrochemical ion gradient to synthesize ATP from ADP and inorganic phosphate (P_i). This key metabolic enzyme uses a unique mechanochemical rotary mechanism to produce the bulk amount of universal energy currency ATP in all living cells, but it is also able to operate in reverse, hydrolyzing ATP, to establish ion gradients by exploiting the energy released from hydrolysis of ATP [1].

In eukaryotes, the ATP synthase is embedded in the inner membrane of mitochondria or in the thylakoid membranes of chloroplasts, while in bacteria and archaea, it is located in the cytoplasmic membrane. In all organisms, the ATP synthase shares an overall highly conserved architecture consisting of a water

soluble F_1 complex (subunits $\alpha_3\beta_3\gamma\delta\epsilon$) and a membrane-intrinsic F_o complex (ab_2c_{8-17}) [2–4] joined together by a central stalk (subunits γ and ϵ) and a peripheral stalk (subunits b_2 and δ). The $\alpha_3\beta_3$ subunits envelop the central stalk γ subunit which by itself introduces an inherent asymmetry into the F_1 headpiece. The lower part of the γ and ϵ subunit is in contact with the membrane-embedded F_o rotor, formed by a number of identical copies of c-subunit, called the c-ring. Recent advances in structural biology have provided new insights into the structure and dynamics of completely assembled complexes of ATP synthase. In particular, it includes also valuable structural information about the previously less well-characterized F_o stator complex in the membrane, its outer stalk region as well as the structural basis of dimerization of

mitochondrial ATP synthases [5–8]. For example, the yeast *Yarrowia lipolytica* F₁F_o-ATP synthase dimer consists of a total of more than 60 different proteins, which in mitochondria form a dimeric ATP synthase of about 1.25 MDa in size and play an important role in the determination of cristae morphology of the inner mitochondrial membrane [8].

From an enzymatic functional point of view, the F₁ complex is the catalytic, ATP-producing or -consuming mechanochemical motor, while the F_o complex represents the electrical motor that generates torque by dissipating the ion gradient by ion translocation. ATP synthesis is driven by the flow of ions through F_o, leading to a rotation of the c-(rotor) ring, which transmits rotation into F₁ via the γ subunit. It is the intrinsically asymmetric γ subunit that finally elicits sequential conformational changes in the three catalytic β subunits, leading to ATP synthesis [9,10].

Inhibitors of ATP synthase have played an important role in the discovery and biochemical characterization of ATP synthases over many decades (for a review, see [11]). The ATP synthesis or hydrolysis can be inhibited by a range of compounds that bind, for example, to the rotor–stator interface region within the F₁ headpiece thereby interfering either with the rotational ATP-synthesizing or ATP-hydrolyzing mechanism, or both [11,12]. Among them is one particular class of natural products, known as polyphenols, which includes stilbene derivatives, such as resveratrol and piceatannol, and flavonoids, such as quercetin (Fig. 1A). Natural polyphenols are found in grapes, peanuts, berries, and red wine. Due to their pharmacokinetic properties and relatively low affinities to human ATP synthases, they are nontoxic at concentrations found in their natural sources. They have been shown to extend the life span of simple organisms [13], but their value in human medicine remains to be determined.

Stilbenes closely resemble the azobenzenes, a very well-established class of synthetic photoswitches [14]. This suggested that the replacement of the stilbene moiety with an isosteric azobenzene (“azologization”) could convert resveratrol and piceatannol into photoswitchable inhibitors whose activity could be turned ON and OFF by light ([15], Fig. 1B). Azobenzenes undergo fast photoisomerization from the thermodynamically more stable, linear *trans* to the more unstable, bent *cis* form

upon irradiation with UV-A or visible light [16]. The *cis* form reverts thermally or can be switched back actively by a different wavelength of light. The wavelength needed for photoisomerization and the rate of thermal reversion can be tuned by modification of the azobenzene chromophore [17,18]. Unlike caged compounds, whose uncaging is irreversible, azobenzenes can be switched ON and OFF repeatedly and over thousands of cycles [16]. They have played a central role in the development of photopharmacology, which is an attempt to control biological function with artificial photoswitches [19–21]. This concept has been applied to biological targets as diverse as ion channels, G-protein coupled receptors, enzymes, and microtubules [22–28].

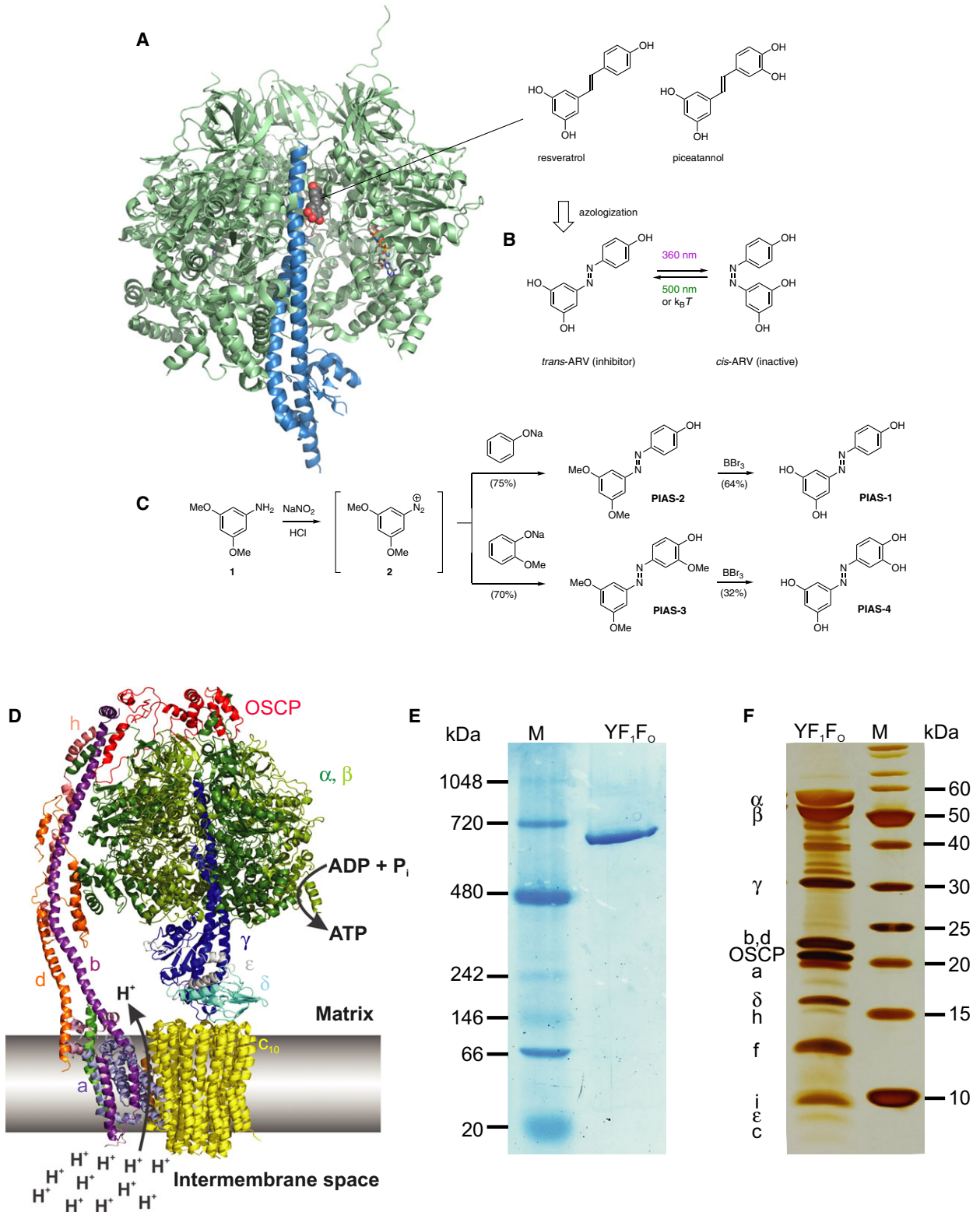
We now report on the extension of photopharmacology to F-type ATP synthases. To this end, we introduce Photoswitchable Inhibitors of ATP Synthase, termed PIAS 1–4 (Fig. 1). We demonstrate that ATP hydrolysis of our test system, the purified yeast *Y. lipolytica* F₁F_o-ATP synthase (Fig. 1D–F), can be optically switched ON and OFF *in vitro* using these molecules. Our results provide a blueprint for the development of precision tools to spatiotemporally control ATP levels and pH gradients in biological systems.

Materials and methods

Chemical synthesis

All reactions of the chemical synthesis of PIAS 1–4 were performed with standard Schlenk techniques under an atmosphere of nitrogen in oven-dried glassware (100 °C oven temperature) that was further dried using a heat gun (set to 650 °C) for all water-sensitive reactions. Dichloromethane (CH₂Cl₂) was distilled from calcium hydride. Reagents were purchased from Sigma-Aldrich (Schnellendorf, Germany), TCI (Eschborn, Germany) or Acros Organics (VWR International GmbH, Darmstadt, Germany) and used without further purification. Reaction progress was monitored by analytical TLC, which was carried out using precoated glass plates (silica gel 60°F₂₅₄) from Merck. Visualization was achieved by exposure to ultraviolet light (UV, 254 nm) where applicable followed by staining with potassium permanganate solution. Flash column chromatography was performed using Merck silica gel (40–63 μ m particle size). Proton NMR (¹H NMR) spectra were recorded on a Varian 300, Varian 400, Inova 400, or Varian 600 spectrometer.

Fig. 1. Design and synthesis of the PIAS. (A) Structure of resveratrol bound to bovine F₁ ATP synthase (from PDB 2JIZ) shown in cartoon representation. Green: α and β subunits of F₁. Blue: γ subunit. The β_{DP} -site containing subunit is removed to provide an unobstructed view of resveratrol wedged between the γ rotor subunit and the α , β stator subunits. Resveratrol (CPK colors, sphere model) is bound in two overlapping orientations. ATP is shown as a stick model in the β_{TP} site. (B) Azologization of resveratrol affords PIAS-1. (C) Chemical synthesis of PIAS-1–4. (D) Cartoon representation of the *Yarrowia lipolytica* F₁F_o ATPase ([8]), and (E) its biochemical characterization by (E) clear native PAGE, Coomassie-stained gel and (F) SDS PAGE, silver-stained gel.



Chemical shifts (δ scale) are expressed in parts per million (p.p.m.) and are calibrated using residual protic solvent as an internal reference (CHCl_3 : $\delta = 7.26$ p.p.m., CD_3OD : $\delta = 3.31$ p.p.m.). Data for ^1H NMR spectra are reported as follows: chemical shift (p.p.m.; multiplicity, coupling constants (Hz), integration). Couplings are expressed as: s = singlet, d = doublet, t = triplet, m = multiplet, or combinations thereof. Carbon NMR (^{13}C NMR) spectra were recorded on the same spectrometers at 75, 100, and 150 MHz (± 1 MHz variance). Carbon chemical shifts (δ scale) are also expressed in p.p.m. and are referenced to the central carbon resonances of the solvents (CDCl_3 : $\delta = 77.16$ p.p.m., CD_3OD : $\delta = 49.00$ p.p.m.). IR spectra were recorded on a Perkin Elmer Spectrum BX II (FTIR System) equipped with an attenuated total reflection (ATR) measuring unit. IR data are reported in frequency of absorption (cm^{-1}). Mass spectroscopy (MS) experiments were performed on a Thermo Finnigan MAT 95 (electron ionization, EI) or on a Thermo Finnigan LTQ FT (electrospray ionization, ESI) instrument.

4-((3,5-dimethoxyphenyl)diazenyl)phenol (PIAS-2)

To an ice-cold solution of 3,5-dimethoxyaniline (306 mg, 2.00 mmol, 1.00 eq.) in THF (5 mL) and HCl (1 M, 6 mL), an aqueous solution (5 mL) of sodium nitrite (166 mg, 2.40 mmol, 1.20 eq.) was added dropwise, resulting in the formation of a dark-red suspension. After 30 min, a solution of phenol (226 mg, 2.40 mmol, 1.20 eq) in aqueous NaOH (1 M, 6 mL) was added dropwise. The mixture was stirred at 0 °C for 1 h before the bulk of the solvent was removed *in vacuo*. The residue was redissolved in ethyl acetate (15 mL) and water (15 mL). After phase separation, the aqueous phase was further extracted with ethyl acetate (3 \times 20 mL). The combined organic layers were washed with water (20 mL) and aqueous saturated sodium chloride (20 mL), then dried over MgSO_4 and concentrated under reduced pressure. Purification by flash column chromatography (5 : 1 hexane: ethyl acetate) afforded PIAS-2 (387 mg, 1.50 mmol, 75%) as a yellow solid.

^1H NMR (400 MHz, CD_3OD) $\delta = 7.81$ – 7.71 (m, 2H), 6.95–6.86 (m, 2H), 6.82 (d, $J = 2.2$, 2H), 6.38 (t, $J = 2.2$, 1H).

HRMS (ESI) m/z calculated for $\text{C}_{14}\text{H}_{15}\text{N}_2\text{O}_3$ 259.1077; found 259.1080. ($\text{M} + \text{H}^+$).

Analytical data were in good agreement with literature values [29].

4-((3,5-dimethoxyphenyl)diazenyl)-2-methoxyphenol (PIAS-3)

To an ice-cold solution of 3,5-dimethoxyaniline (306 mg, 2.00 mmol, 1.00 eq.) in THF (5 mL) and HCl (1 M, 6 mL), an aqueous solution (5 mL) of sodium nitrite (166 mg, 2.40 mmol, 1.20 eq.) was added dropwise, resulting in the formation of a dark-red suspension. After 30 min, a solution of guaiacol (298 mg, 2.40 mmol, 1.20 eq) in aqueous NaOH (1 M, 6 mL) was added dropwise. The mixture was stirred at

0 °C for 1 h before the bulk of the solvent was removed *in vacuo*. The residue was redissolved in ethyl acetate (15 mL) and water (15 mL). After phase separation, the aqueous phase was further extracted with ethyl acetate (3 \times 20 mL). The combined organic layers were washed with water (20 mL) and aqueous saturated sodium chloride (20 mL), then dried over MgSO_4 and concentrated under reduced pressure. Purification by flash column chromatography (5 : 1 hexane : ethyl acetate) afforded PIAS-3 (243 mg, 1.40 mmol, 70%) as a yellow solid.

^1H NMR (400 MHz, CDCl_3) $\delta = 7.61$ (dt, $J = 8.4$, 1.5, 1H), 7.50 (t, $J = 1.5$, 1H), 7.10–7.08 (m, 2H), 7.06 (dd, $J = 8.4$, 1.1, 1H), 6.57 (q, $J = 2.0$, 1H), 5.95 (s, 1H), 4.00 (d, $J = 1.1$, 3H), 3.88 (d, $J = 1.1$, 6H).

HRMS (ESI) m/z calculated for $\text{C}_{15}\text{H}_{17}\text{O}_4\text{N}_2$ 289.1183; found 289.1187 ($\text{M} + \text{H}^+$).

Analytical data were in good agreement with literature values [29].

5-((4-hydroxyphenyl)diazenyl)benzene-1,3-diol (PIAS-1)

To a solution of dimethyl PIAS-2 (77 mg, 0.30 mmol, 1.00 eq) in CH_2Cl_2 (8 mL), boron tribromide solution was added in CH_2Cl_2 (1.0 M, 2.1 mL, 2.1 mmol, 7.0 eq) dropwise at 0 °C. After warming to room temperature over 14 h, liquid chromatography–mass spectrometry (LC-MS) analysis indicated full conversion. Saturated aq. NaHCO_3 (15 mL) was added at room temperature and the mixture was poured on water (10 mL). After extraction of the aq. phase with EtOAc (4 \times 20 mL), the combined organic phases were washed with aqueous saturated sodium chloride (20 mL), dried and evaporated to give a black oil that was purified by column chromatography (9 : 1 CH_2Cl_2 : MeOH) to give PIAS-1 as a dark-red solid (44 mg, 0.19 mmol, 64%).

^1H NMR (400 MHz, CD_3OD) $\delta = 7.81$ – 7.71 (m, 2H), 6.95–6.86 (m, 2H), 6.82 (d, $J = 2.2$, 2H), 6.38 (t, $J = 2.2$, 1H).

HRMS (ESI) m/z calculated for $\text{C}_{12}\text{H}_{10}\text{O}_3\text{N}_2$ 231.0764; found 231.0763 ($\text{M} + \text{H}^+$).

Analytical data were in good agreement with literature values [29].

4-((3,5-dihydroxyphenyl)diazenyl)benzene-1,2-diol (PIAS-4)

To a solution of PIAS-3 (115 mg, 0.40 mmol, 1.00 eq) in CH_2Cl_2 (8 mL), boron tribromide solution was added in CH_2Cl_2 (1.0 M, 3.6 mL, 3.6 mmol, 9.0 eq) dropwise at 0 °C. After warming to room temperature over 14 h, LC-MS analysis indicated full conversion. Saturated aq. NaHCO_3 (15 mL) was added at room temperature and the mixture was poured on water (10 mL). After extraction of the aq. phase with EtOAc (4 \times 20 mL), the combined organic phases were washed with aqueous saturated sodium chloride

(20 mL), dried and evaporated to give a black oil that was purified by column chromatography (9 : 1 CH₂Cl₂ : MeOH) to give PIAS-4 as a dark-red amorphous solid (32 mg, 0.13 mmol, 32%).

R_f 0.52 (water : MeOH 3 : 2).

¹H NMR (400 MHz, CD₃OD) δ = 7.37–7.33 (m, 2H), 6.92–6.88 (m, 1H), 6.79 (d, *J* = 2.2, 2H), 6.37 (t, *J* = 2.2, 1H).

¹³C NMR (101 MHz, CD₃OD) δ = 160.0, 156.1, 150.4, 147.7, 147.0, 120.2, 115.9, 107.6, 105.4, 102.1.

IR (ATR) 3258, 1675, 1601, 1379, 1284, 1156, 1001 cm⁻¹.

HRMS (ESI) *m/z* calculated for C₁₂H₁₁O₄N₂ 247.0641; found 247.0713.

See Figs S3 and S4 for NMR spectra of PIAS-4.

Purification of *Yarrowia lipolytica* F₁F_o-ATP synthase

Monomeric form of *Y. lipolytica* F₁F_o-ATP synthase was purified as described in [8]. Briefly, the ATP synthase was isolated from mitochondria prepared from large-scale *Y. lipolytica* cultures [30]. The isolation, solubilization, and collection of solubilized material from mitochondrial membranes were carried out as previously described [31]. After the removal of complex I by metal affinity purification [31], glycerol was added to a final concentration of 20% (v/v) to the solubilized membranes, which were rapidly frozen in liquid nitrogen for storage at –80 °C. The solubilize was thawed on ice and supplied with 50 mM MgCl₂. To the slow stirring suspension on ice, 3% (w/w) polyethylene glycol (PEG) 6000 was added from a 50% (w/w) stock solution to induce protein precipitation. After 15 min of continued stirring on ice, the precipitated proteins were removed by centrifugation (15 min and 20 000 *g* at 4 °C). The ATP synthase-containing fraction was then precipitated by the increase in the polyethylene glycol 6000 concentration to 6% (w/w), again with continuous stirring on ice for 15 min and then collected by centrifugation for 15 min, 20 000 *g* at 4 °C. The pellet was then dissolved in 2 mL of buffer A [30 mM 3-(*N*-morpholino)-propanesulfonic acid (MOPS/NaOH pH 7.4), 4 mM MgCl₂, 2 mM EDTA and 0.1% (w/v) DDM], the sample was applied on a density-based discontinuous glycerol gradient (1 mL steps with 15, 20, 25, 28, 30, 35, 40, 45, 50% glycerol in buffer A) and run for 16 h at 4 °C and at 151 177 *g* in a SW40 rotor (Beckman Coulter, Indianapolis, IN, USA). After the run, 1 mL fractions were collected from top using a pipette and the ATP synthase-containing fractions, as judged by high-resolution Clear Native PAGE (hrCN-PAGE [32]), were pooled and directly loaded onto an anion exchange chromatography using a POROS GoPure HQ 50 anion exchange column (Life Technologies, ThermoFisher Scientific, Waltham, MA, USA), which was previously equilibrated with one column volume (CV) of buffer A, using an ÄKTAexplorer chromatography

system (GE Healthcare, Munich, Germany). The column was then washed with 1 CV of buffer A and the *Y. lipolytica* ATP synthase was eluted by a continuous gradient using buffer B (buffer A with 1 M NaCl). The ATP synthase as judged by high-resolution Clear Native PAGE (hrCN-PAGE [32]) was concentrated to 1 mg·mL⁻¹ by ultrafiltration using Vivaspin PES membranes with a molecular weight cutoff of 100 kDa at 1500 *g* and 4 °C to 2 mL final volume. The protein concentration was determined using the bicinchoninic acid (BCA) method (Pierce; ThermoFisher Scientific). Bovine serum albumin was used as a standard between 2 and 2000 µg·mL⁻¹.

Determination of ATP hydrolysis activity using the malachite green assay

The ATP hydrolysis activity was determined using the malachite green assay as described in [33–35]. Briefly, 1 mg·mL⁻¹ *Y. lipolytica* ATP synthase protein solution was prepared in a reaction tube and supplemented with 10 µg·mL⁻¹ cardiolipin and 40 µg·mL⁻¹ yeast extract lipids and diluted in the reaction buffer (50 mM Tricine-NaOH pH 8.0, 5 mM MgCl₂; 150 µL per experiment). The malachite green stock reagent (320 µL per experiment) was prepared [0.08% (w/v) malachite green: 2.3% (v/v) polyvinyl alcohol: 5.7% (w/v) ammonium molybdate: 6 N HCl in distilled water (ratio 2 : 1 : 1 : 2)] and incubated for 30 min at room temperature before use. A time course for ATPase activity was measured, taking sample aliquots from the reaction tube and stopping the reaction after four time points, in 1-min intervals: Each reaction was started by the addition of 5 mM Na₂-ATP (pH 7.4) using a 0.2 M stock solution. At each taken time point, an aliquot of 20 µL of reaction mix was transferred into 80 µL malachite green reagent and immediately mixed. After 75 seconds, each reaction was quenched by the addition of 34% (w/v) sodium citrate. Each time course was measured in triplicates; a calibration curve (0, 3, 6, and 12 nmol P_i) was determined in duplicates for each measurement. Note: The malachite green assay is a colorimetric method for measuring P_i in aqueous solutions and was performed on aliquots taken from the reaction tube. As such, it does not interfere with photoswitching. Conversely, the azobenzene has no absorption beyond 600 nm, which could potentially falsify the assay.

Inhibition of ATP hydrolysis activity by resveratrol and PIAS 1–4

PIAS 1–4 stock solutions (concentrations: 0.01, 0.1, 0.5, 5, 10, 20, and 50 mM, dissolved in methanol) and resveratrol (concentration 0.01, 0.1, 0.5, 5, 10, 50, and 100 mM (Sigma-Aldrich, D) in pure ethanol were diluted to 1% (v/v) and added to the *Y. lipolytica* ATP synthase sample (1 mg·mL⁻¹ diluted 1/100 in reaction buffer) and incubated at room temperature for 1 h. As a control, 1% (v/v) of

methanol/ethanol was added only. The ATP hydrolysis activities were then determined using the malachite green assay. To next study the effect of UV irradiation on the samples containing the azo-compounds (absorption maxima at 365 nm) and their effect on the change in ATP hydrolysis activity due to UV irradiation, the UV irradiation experiments were performed the following way: a 365-nm laser [Thorlabs (Dachau/Munich, Germany) M365L2-UV (365 nm) mounted LED, 700 mA, 190 mW (min)] was used to constantly irradiate the reaction mix in each sample in the cuvette at a distance of 91.4 mm in a homemade setup as shown in Fig. S1. The irradiation time for the whole reaction time is 4 min. After that, the malachite green assay was performed the same as described for nonirradiated samples. Table S1 shows the results of each measurement before and after irradiation.

Statistical analysis

The results (Fig. 3) were represented as the mean \pm SEM of the three replicates from three independent experiments ($n = 9$). A calibration curve for the absorption/ P_i was generated to calculate the P_i concentration at each time point (P_i /time) from the absorption of the malachite green complex at 620 nm (absorption/time). The P_i concentration per time corresponds to the ATP hydrolysis activity in Units/min. The percentage of inhibition was determined by normalizing the ATP hydrolysis activity of solutions with inhibitors with the native, monomeric *Y. lipolytica* ATP hydrolytic enzyme's activity. The values of the inhibitor concentration at which 50% of the ATP hydrolysis activity was inhibited (IC_{50} values) were calculated using GRAPHPAD PRISM® 5, version 5.01 (GraphPad Software, Inc., San Diego, CA, USA) by plotting the log concentration of the azo compounds versus the percentage inhibition of ATP hydrolysis activities.

Results

Design, synthesis and photophysical characterization of the PIAS

The design of the PIAS was based on an X-ray crystal structure of the bovine mitochondrial ATP synthase in complex with resveratrol, piceatannol, and quercetin (Fig. 1). According to this structure, the polyphenols bind in a hydrophobic pocket between the rotor γ subunit C-terminal end and the surrounding region formed by the stator α and β subunits (Fig. 1A, [36]). This interaction blocks the rotation of the rotor against the stator and thereby catalysis. Accordingly, we reasoned that the PIAS inhibit the ATPase in their *trans* form, which closely resembles the polyphenols, and remain inactive in their bent *cis* form (Fig. 1B),

which could not be accommodated in the sleeve-like binding site defined by the X-ray crystal structure.

The synthesis of PIAS 1–4 by azo coupling is shown in Fig. 1C. Diazotization of 3,5-dimethoxyaniline (**1**) gave the diazonium salt **2**, which was treated *in situ* with the sodium salt of either phenol or guaiacol to give PIAS-2 and PIAS-3 in 75% and 70% yield, respectively. Global demethylation using excess boron tribromide in CH_2Cl_2 yielded PIAS-1, an azolog of resveratrol, and PIAS-4, an azolog of piceatannol, in 64% and 32% yield, respectively. PIAS 1–3 had previously been prepared by a similar sequence [29].

All four compounds ($\geq 95\%$ pure by 1H NMR) showed comparable absorption maxima between 340 and 360 nm in acetonitrile/water solution. No isomerization to the *cis* isomer was apparent upon irradiation with 365 nm even with high-power LED light. This is due to the known very fast thermal relaxation of azobenzenes that bear a *para*-hydroxy group [37,38]. In the dark as well as under ambient light conditions, we could only observe the *trans* isomer using 1H NMR spectroscopy. The photostationary states of the PIAS under physiological conditions could not be determined directly for the same reason.

Choice of *Yarrowia lipolytica* ATP synthase as test system

The crystal structure of *trans*-resveratrol and *trans*-piceatannol in complex with the bovine F-type ATPase shows a distinct binding pocket for polyphenols formed between an α -subunit, the β_{TP} -subunit and the C-terminal part of the γ subunit (Fig. 1A, [36]). The residues of the binding pocket of polyphenols in the bovine enzyme are well conserved both within eukaryotic and bacterial types of ATP synthases (Fig. S2, alignment), suggesting that they harbor an identical binding pocket in the *Y. lipolytica* ATP synthase except for three amino acids in the γ subunit of which two ($\gamma I263V$ and $\gamma E264D$) are conservative, and in the case of $\gamma K260N$, the interaction occurs via hydrophobic interactions, while the positively charged nitrogen points away from the resveratrol molecule. Given that and the fact that the purification procedure of *Y. lipolytica* ATP synthase was already available in our laboratory [8], we decided to use this ATPase as a model system to study the effect of the PIAS on the ATPase hydrolytic activity. First, the fully assembled, monomeric form of *Y. lipolytica* ATP synthase was purified (Fig. 1D–F). Then, the ATP hydrolysis activity of the enzyme was determined to be $7 U \cdot mg^{-1}$ with a variance of $3 U \cdot mg^{-1}$ due to three biological replicates measured.

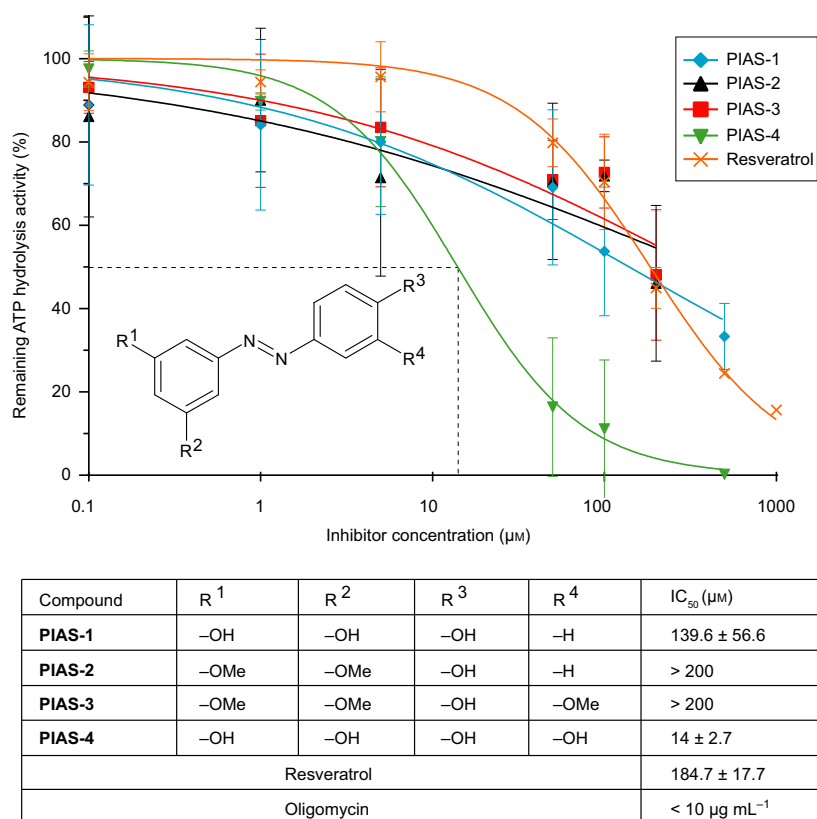


Fig. 2. Inhibition of ATPase activity of *Yarrowia lipolytica* F₁F₀-ATP synthase by PIAS 1–4. The inhibition of the ATP hydrolysis activity by PIAS 1–4 was determined using the malachite green assay. The results of the ATP hydrolysis activity measurements were plotted and fitted against the inhibitor concentration. The IC₅₀ values are listed below in the table. Each measurement was done in triplicates and three biological replicates.

The measured activities are well in the range of reported literature values [8]. To test the F₁-F₀ coupled activity of the enzyme, we used the inhibitor oligomycin, which showed that 95 ± 5% of this ATPase's activity could be inhibited [39].

Inhibition of *Y. lipolytica* ATP hydrolysis activity by resveratrol and *trans*-PIAS 1–4

Using the fully active, coupled ATP synthase from *Y. lipolytica*, we next tested the capability of resveratrol and resveratrol derivatives, PIAS 1–4, to inhibit the ATPase activity in a concentration-dependent manner and with all compounds in their *trans* form (Fig. 2). First, the control experiment was performed, using resveratrol at concentrations from 0.1 to 1 mM. Resveratrol was able to reduce the ATP hydrolytic-specific activity to 1.4 U·mg⁻¹, corresponding to 16% of the initially uninhibited activity. The inhibition experiments were then performed using different concentrations from 0.1 to 200 μM (PIAS-1, PIAS-4) and 0.1 to 500 μM (PIAS-2–3) and the inhibitory concentration that

inhibits 50% of the initial activity (IC₅₀) was calculated and determined, showing an IC₅₀ of 184.7 ± 17.7 μM for resveratrol in the *Y. lipolytica* ATP synthase.

Furthermore, all four PIAS showed a concentration-dependent inhibitory effect on ATP hydrolysis activity, however to various degrees. Among these derivatives, PIAS-4, the azo-polyphenol with an additional hydroxy group (R₄=OH) was the most potent inhibitor, showing 100% ATPase inhibition at a concentration of 500 μM (IC₅₀ = 14 ± 2.7 μM). PIAS-1, the azo-resveratrol derivative, was less potent and inhibited the ATPase with an IC₅₀ = 139.6 ± 56.6 μM. The methylated derivatives PIAS-2 and PIAS-3, finally, showed the lowest inhibitory activity, with an IC₅₀ above 200 μM in both cases.

Optical control of ATP synthase activity *in vitro*

The PIAS derivatives undergo an isomerization from the stable *trans* isomer to the *cis* isomer upon irradiation with UV-A light (Fig. 1B,C). Next, to study the impact of the *cis* isomers on ATPase, we used a

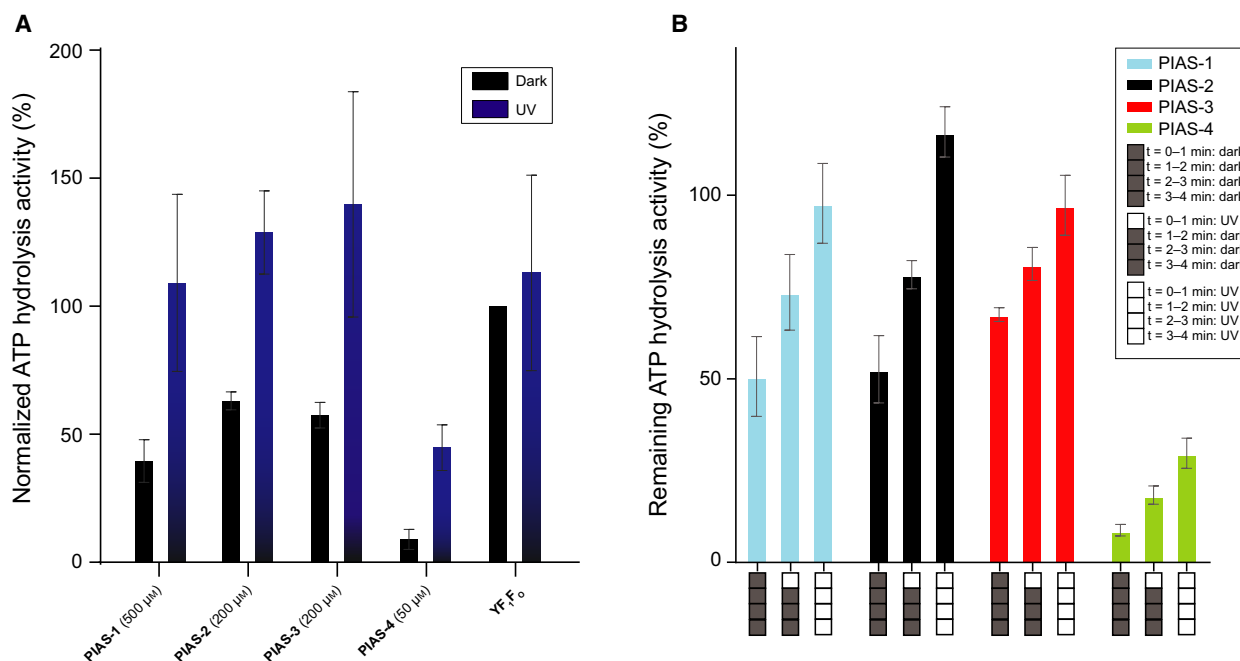


Fig. 3. Optical control of ATPase activity *in vitro* using purified *Yarrowia lipolytica* ATP synthase (A) and reversibility (B). For each measurement, a sample of $0.01 \text{ mg}\cdot\text{mL}^{-1}$ ATP synthase in the reaction buffer was used to measure the initial ATP-hydrolytic activity. The activities were normalized against the *Y. lipolytica* F₁F_o ATPase activity under dark conditions. The ATPase activity was inhibited by adding (1) 500 μM , (2) 200 μM , (3) 200 μM , (4) 50 μM of compound PIAS-1, 2, 3, and 4, respectively. All concentrations used were higher than the previously determined IC₅₀ for each compound. The reactions were activated by switching UV laser light (365 nm) for 3 min at room temperature. The ATP hydrolysis activity was determined by the malachite green assay and normalized against the ATP hydrolysis activity of the native enzyme without UV irradiation. All compounds showed an inhibitory effect on ATP hydrolysis activity under dark conditions, which could be reduced by UV-A irradiation. The assays were repeated four times and performed in triplicates. (B) For each inhibitor, measured series were performed under dark conditions (indicated by four black boxes), 1-min UV irradiation followed by 3-min dark conditions (one white box, three black boxes) and continuous UV-A irradiation (four white boxes). The measurement was performed similar to the UV measurement shown in Fig. 3A, apart from the UV irradiation times. The ATP hydrolysis activity was determined by the malachite green assay and normalized against the ATP hydrolysis activity of the native enzyme without UV irradiation. All compounds showed inhibition of ATP hydrolysis activity under dark conditions, higher activities with 1-min UV irradiation and the highest activity in case of 4-min UV irradiation. The assays were repeated three times and performed in triplicates.

190 mW (Min) UV-A laser at a wavelength of 365 nm to irradiate the samples for 3 min and determined their ATP hydrolysis activity shortly thereafter (Fig. S1). The PIAS concentrations were chosen (PIAS-1: 500 μM , PIAS-2–3: 200 μM , and PIAS-4: 50 μM) according to their previously determined IC₅₀ values. The chosen concentrations should ensure inhibition up to 60% while not blocking ATP hydrolysis completely, to be able to observe photo-switching effects (Fig. 3A). While the nonirradiated PIAS-1–4 inhibited the *Y. lipolytica* ATP hydrolysis activities to different degrees, the samples irradiated with 365 nm light showed a reduced capability to inhibit the ATPase hydrolytic activity, comparable to the yeast wild-type sample (compare purple columns of PIAS 1–4 with YF₁F_o in Fig. 3A). Specifically, the nonirradiated PIAS-4 inhibited ATP hydrolysis activity best and up to 90% at 50 μM after 3 min

(black column of PIAS-4 in Fig. 3A), while irradiated for 3 min, PIAS-4 lost its potency for inhibition and showed only 55% of ATP hydrolysis inhibition (purple column of PIAS-4 and YF₁F_o in Fig. 3A). Remarkably, while all other three PIAS compounds (PIAS-1, PIAS-2, and PIAS-3) were less potent in ATPase inhibition, they were able to regain the full level of wild-type activity, showing no more inhibitory effect (purple columns of PIAS-1–3 compared with YF₁F_o in Fig. 3A). Hence, the 3-min irradiation procedure completely abrogated their capability to inhibit ATPase.

ATPase activity can be reversibly controlled by light

Next, we determined to what extent the described effect of PIAS 1–4 on ATP hydrolysis activity can be

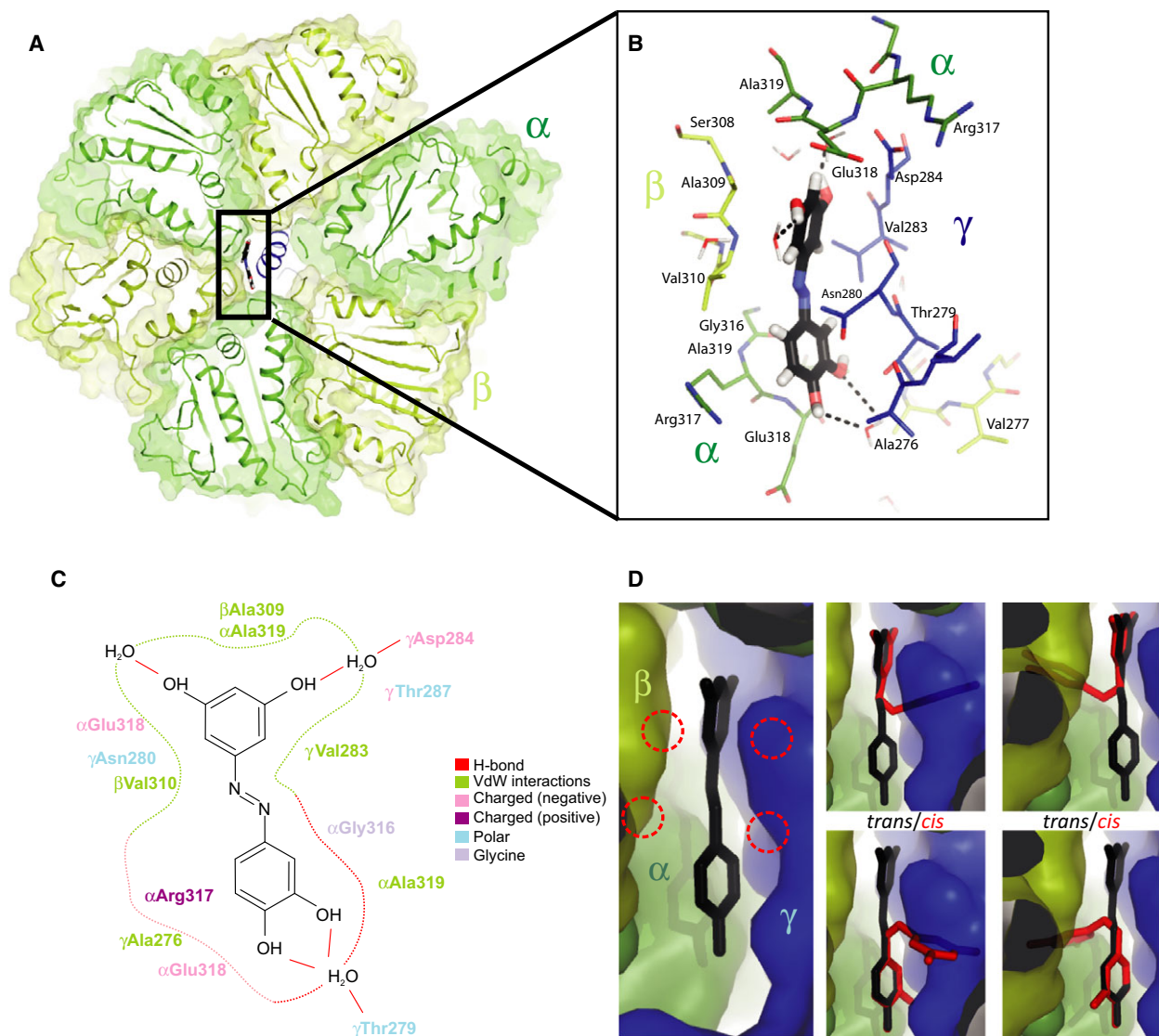


Fig. 4. Model PIAS-1 bound to the *Yarrowia lipolytica* F₁ ATPase domain. The bovine F₁-resveratrol structure (pdb ID 2jiz, [36]) was used to create a model with the *Y. lipolytica* ATPase (pdb ID 5fl7, [8]) and the azo-polyphenols used in this study. Colors: α dark green, β light green, γ blue (A) Tilted view into the F₁-ATPase upward from the inner mitochondrial membrane. The azo-resveratrol (stick representation, highlighted by a black box) binds in a pocket made by the subunits α , β , and γ . (B) Zoom [boxed in (A)] to interaction site of azo-polyphenol bound to the F₁-ATPase. Hydrogen bonds are indicated by black dashed lines. (C) Two-dimensional interaction plot of the azo-polyphenol interaction with the F₁-ATPase (created using Maestro [41]). Interaction distances are color coded. The interaction network of the polyphenol hydrogen bonds as well as hydrophobic and polar interactions contribute to the binding affinity of the polyphenol. (D) Modeling of *cis*- and *trans*-polyphenols in F₁ ATPase. Left panel: Side view of resveratrol-F₁ binding pocket. Various orientations of *cis*-polyphenols (in red) are modeled and shown in the four right panels along with the *trans*-configurations (black). All *cis*-molecules generate steric clashes with the Van der Waals radii of the F₁ subunits, indicated by the dashed circles in the left panel.

reversed to restore ATPase activity (Fig. 3B). To test this, we used an irradiation protocol that was applied on three differently treated 1 μ g samples of *Y. lipolytica* ATPase: the first sample was kept in the dark for 4 min, the second sample was irradiated for just 1 min followed by 3 min in the dark, and the third sample was irradiated continuously for 4 min. After these

treatments, the ATPase activity was determined (Fig. 3B). Generally, all compounds, PIAS 1–4, showed the lowest effects on ATP hydrolysis activity while being in the dark (Fig. 3B; 0–4 min: dark) but the highest ATPase activities upon continuous UV irradiation (Fig. 3B; 0–4 min: UV). Remarkably, ATP hydrolysis activity for the measured samples with 1-

min irradiation (Fig. 3B; 0–1 min UV, 1–4 min: dark) is lower than the activity for the measured samples with 4-min irradiation time, which exemplifies the reversibility of ATPase inhibition using PIAS 1–4.

The observed results can be rationalized the following way: The PIAS 1–4 compounds in the *cis* conformation do not inhibit the ATP hydrolysis activity during the first minute of irradiation; however, they all isomerize back into their *trans*-isoforms under dark conditions. It is this *trans*-isoform in which PIAS 1–4 are again capable of inhibiting the enzyme. The differences in ATP hydrolysis activities for the three measured samples using PIAS 1–4 are due to their different potency to inhibit the ATPase: PIAS-4 inhibits up to 90% under dark conditions, ~80% with 1-min irradiation and 65% with continuous irradiation, while the nonirradiated PIAS 1–3 inhibit between 40% and 50%, between 20% and 30% with 1-min irradiation and do not show any inhibition effect under continuous irradiation.

Discussion

This study reports about the synthesis of new, reversible photoswitches derived from natural stilbenoid polyphenols such as resveratrol, for the optical control of the yeast *Y. lipolytica* ATPase activity. Resveratrol itself can be photoisomerized, but this requires short, cytotoxic wavelengths (< 300 nm) and eventually results in the formation of a photochemical byproduct (resveratrone) [40]. We therefore synthesized four azobenzenes, PIAS 1–4, and evaluated them for their ability to reversibly inhibit ATPase activity, with resveratrol as reference inhibitor. The *trans*-isomers indeed inhibit the ATP hydrolytic activity, while isomerization to the *cis* isomers decreased enzymatic activity inhibition. The study also demonstrates that PIAS-1–4 can be used as reversible ON/OFF switches for *Y. lipolytica* ATPase.

The high-sequence homology between bovine and yeast *Y. lipolytica* ATPase and the isosteric nature of resveratrol and *trans*-PIAS-1 suggests that the molecular mechanism of binding and ATPase inhibition of the two compounds is identical. To support this notion, we further explored this possibility with molecular modeling using Maestro ([41], Fig. 4C). The template yeast F₁-PIAS-4 bound structure used for the molecular modeling was created in Pymol [42] by merging the bovine F₁-resveratrol structure (pdb ID 2jiz, [36]) with the *Y. lipolytica* ATPase (pdb ID 5fl7, [8]) and PIAS-4. Our model of *trans*-PIAS-4 bound to the *Y. lipolytica* enzyme shows hydrophobic interactions of the azobenzene with residues from three

different subunits of the F₁ complex. The residues γ V283, β_{TP} V310, and β_{TP} A309 are equivalent to residues γ I263, β_{TP} V279, and β_{TP} A278 in bovine F₁. Additionally, nonpolar interactions are formed by side chains that involve the two residues α A319 and γ A276. The *trans*-PIAS-4 binding to the *Y. lipolytica* F₁ complex appears to be further stabilized by a hydrogen bond network involving the hydroxy groups of *trans*-PIAS-4 and F₁ complex intrinsic water molecules. It has been shown in purified *Escherichia coli* F₁ and F₁F_o ATPase in membrane vesicles that the relative positions of hydroxy groups of polyphenols appear to be critical for the degree of inhibition of ATPase hydrolysis [43]. The four compounds PIAS 1–4, which have either methoxy or hydroxy groups at positions 1–4 inhibited the *Y. lipolytica* ATP synthase to different degrees. Given that and the findings made for the *E. coli* ATPase, we therefore suggest that the bulkier methoxy groups of PIAS-2 and PIAS-3 at positions 2 and 3 provide a rationale to understand the decreased inhibitory effects on *Y. lipolytica* ATP synthase by these two compounds. Their larger side chains may cause steric hindrance in the inhibitor-binding site (Fig. 4D). Without further experimental structural information available, one cannot exclude the alternative possibility that decreased inhibition results from the absence of hydrogen bond donors at the ligand sites R1, R2, and R4.

While our studies were ongoing, Hoersch published the optical control of *E. coli* F₁-ATPase using a photoswitchable cross linker [44]. Crosslinking with an azobenzene bismaleimide between engineered cysteines in the α - and β -subunits reduced the ATP hydrolysis activity in a light-dependent fashion. This approach requires genetic engineering of the ATPase and covalent attachment with maleimides. In contrast, our study uses the complete and genetically unmodified, native F₁F_o ATP synthase holoenzyme (Fig. 1D–F); hence, it has the potential to be used with broader applicability, for example, in genetically nonmodified host cells.

Finally, our work extends the reach of photopharmacology to an important new target class and provides a blueprint for the development of photoswitches that enable to spatiotemporally control ATP-dependent reactions, for example, in *in vitro* biotechnological applications. The exact mechanism by which resveratrol promotes a wide range of beneficial effects in humans is still unclear. As PIAS 1–4 inhibit ATPase in an analogous fashion, future photochemical experiments with the PIAS on other resveratrol targets and pathways such as AMPK and SIRT1, which are the key metabolic effectors of resveratrol, could provide

more insights on the fundamental biochemical actions of resveratrol. This work could be explored to other resveratrol targets such as cyclooxygenases [45], phosphodiesterases [46], and estrogen receptors [47]. PIAS-1 and PIAS-4 provide a proof of principle and a basis for further chemical modifications that potentially can fulfill the requirements of *in vivo* studies, for example, high-binding affinities and mitochondrial-targeting motifs. As the studied PIAS activities can be switched off, future work could shed more light on the molecular mechanisms governing the biochemical properties of resveratrol.

Acknowledgements

We thank Jürgen Reichert (Max-Planck-Institute of Biophysics, Frankfurt am Main, Germany) who designed and constructed the device for the UV measurements (Fig. S1). We also thank Werner Kühlbrandt for his support and lab space. This work was financially supported by the Deutsche Forschungsgemeinschaft (SFB 807 and SFB 1032) and the Wellcome Trust (WT110068/Z/15/Z).

Author contributions

TM and DT conceived and directed the study. BE designed and carried out biological experiments and analyzed data; FH designed and carried out chemical syntheses. All authors contributed to writing the manuscript.

References

- Junge W, Nelson N (2015) ATP synthase. *Annu Rev Biochem* **84**, 631–657.
- Meier T, Faraldo-Gómez JD and Börsch M (2011) ATP Synthase – A Paradigmatic Molecular Machine. In *Molecular Machines in Biology: Workshop of the Cell* (Frank J, ed), pp. 208–238. Cambridge University Press, Cambridge.
- Schulz S, Wilkes M, Mills DJ, Kuhlbrandt W and Meier T (2017) Molecular architecture of the N-type ATPase rotor ring from *Burkholderia pseudomallei*. *EMBO Rep* **18**, 526–535.
- Watt IN, Montgomery MG, Runswick MJ, Leslie AGW and Walker JE (2010) Bioenergetic cost of making an adenosine triphosphate molecule in animal mitochondria. *Proc Natl Acad Sci USA* **107**, 16823–16827.
- Allegretti M, Klusch N, Mills DJ, Vonck J, Kühlbrandt W and Davies KM (2015) Horizontal membrane-intrinsic alpha-helices in the stator a-subunit of an F-type ATP synthase. *Nature* **521**, 237–240.
- Morales-Rios E, Montgomery MG, Leslie AGW and Walker JE (2015) Structure of ATP synthase from *Paracoccus denitrificans* determined by X-ray crystallography at 4.0 Å resolution. *Proc Natl Acad Sci USA* **112**, 13231–13236.
- Zhou A, Rohou A, Schep DG, Bason JV, Montgomery MG, Walker JE, Grigorieff N and Rubinstein JL (2015) Structure and conformational states of the bovine mitochondrial ATP synthase by cryo-EM. *Elife* **4**, e10180.
- Hahn A, Parey K, Bublitz M, Mills Deryck J, Zickermann V, Vonck J, Kühlbrandt W and Meier T (2016) Structure of a complete ATP synthase dimer reveals the molecular basis of inner mitochondrial membrane morphology. *Mol Cell* **63**, 445–456.
- Abrahams JP, Leslie AGW, Lutter R and Walker JE (1994) Structure at 2.8 Å resolution of F₁-ATPase from bovine heart mitochondria. *Nature* **370**, 621–628.
- Boyer PD (1997) The ATP synthase—a splendid molecular machine. *Annu Rev Biochem* **66**, 717–749.
- Hong S and Pedersen PL (2008) ATP synthase and the actions of inhibitors utilized to study its roles in human health, disease, and other scientific areas. *Microbiol Mol Biol Rev* **72**, 590–641.
- Gledhill JR and Walker JE (2006) Inhibitors of the catalytic domain of mitochondrial ATP synthase. *Biochem Soc Trans* **34**, 989–992.
- Bhullar KS and Hubbard BP (2015) Lifespan and healthspan extension by resveratrol. *Biochim Biophys Acta* **1852**, 1209–1218.
- Szymański W, Beierle JM, Kistemaker HAV, Velema WA and Feringa BL (2013) Reversible photocontrol of biological systems by the incorporation of molecular photoswitches. *Chem Rev* **113**, 6114–6178.
- Schoenberger M, Damijonaitis A, Zhang Z, Nagel D and Trauner D (2014) Development of a new photochromic ion channel blocker via azologization of fomocaine. *ACS Chem Neurosci* **5**, 514–518.
- Bandara HMD and Burdette SC (2012) Photoisomerization in different classes of azobenzene. *Chem Soc Rev* **41**, 1809–1825.
- Dong M, Babalhavaeji A, Samanta S, Beharry AA and Woolley GA (2015) Red-shifting azobenzene photoswitches for *in vivo* use. *Acc Chem Res* **48**, 2662–2670.
- Konrad DB, Frank JA and Trauner D (2016) Synthesis of redshifted azobenzene photoswitches by late-stage functionalization. *Chem Eur J* **22**, 4364–4368.
- Broichhagen J, Frank JA and Trauner D (2015) A roadmap to success in photopharmacology. *Acc Chem Res* **48**, 1947–1960.
- Lerch MM, Hansen MJ, van Dam GM, Szymanski W and Feringa BL (2016) Emerging targets in

- photopharmacology. *Angew Chem Int Ed Engl* **55**, 10978–10999.
- 21 Velema WA, Szymanski W and Feringa BL (2014) Photopharmacology: beyond proof of principle. *J Am Chem Soc* **136**, 2178–2191.
- 22 Borowiak M, Nahaboo W, Reynders M, Nekolla K, Jalinet P, Hasserodt J, Rehberg M, Delattre M, Zahler S, Vollmar A *et al.* (2015) Photoswitchable inhibitors of microtubule dynamics optically control mitosis and cell death. *Cell* **162**, 403–411.
- 23 Frank JA, Yushchenko DA, Hodson DJ, Lipstein N, Nagpal J, Rutter GA, Rhee JS, Gottschalk A, Brose N, Schultz C *et al.* (2016) Photoswitchable diacylglycerols enable optical control of protein kinase C. *Nat Chem Biol* **12**, 755–762.
- 24 Hartrampf FWW, Barber DM, Gottschling K, Leippe P, Hollmann M and Trauner D (2017) Development of a photoswitchable antagonist of NMDA receptors. *Tetrahedron* **73**, 4905.
- 25 Laprell L, Repak E, Franckevicius V, Hartrampf F, Terhag J, Hollmann M, Sumser M, Rebola N, DiGregorio DA and Trauner D (2015) Optical control of NMDA receptors with a diffusible photoswitch. *Nat Commun* **6**, 8076.
- 26 Pittolo S, Gómez-Santacana X, Eckelt K, Rovira X, Dalton J, Goudet C, Pin JP, Llobet A, Giraldo J, Llebaria A *et al.* (2014) An allosteric modulator to control endogenous G protein-coupled receptors with light. *Nat Chem Biol* **10**, 813–815.
- 27 Reis SA, Ghosh B, Hendricks JA, Szantai-Kis DM, Türk L, Ross KN, Lamb J, Read-Button W, Zheng B, Wang H *et al.* (2016) Light-controlled modulation of gene expression by chemical optoepigenetic probes. *Nat Chem Biol* **12**, 317–323.
- 28 Szymanski W, Ourailidou ME, Velema WA, Dekker FJ and Feringa BL (2015) Light-controlled histone deacetylase (HDAC) inhibitors: towards photopharmacological chemotherapy. *Chem Eur J* **21**, 16517–16524.
- 29 Song YM, Ha YM, Kim JA, Chung KW, Uehara Y, Lee KJ, Chun P, Byun Y, Chung HY and Moon HR (2012) Synthesis of novel azo-resveratrol, azo-oxresveratrol and their derivatives as potent tyrosinase inhibitors. *Bioorg Med Chem Lett* **22**, 7451–7455.
- 30 Kashani-Poor N, Kerscher S, Zickermann V and Brandt U (2001) Efficient large scale purification of his-tagged proton translocating NADH:ubiquinone oxidoreductase (complex I) from the strictly aerobic yeast *Yarrowia lipolytica*. *Biochim Biophys Acta* **1504**, 363–370.
- 31 Hunte C, Zickermann V and Brandt U (2010) Functional modules and structural basis of conformational coupling in mitochondrial complex I. *Science* **329**, 448–451.
- 32 Ladig R, Sommer MS, Hahn A, Leisegang MS, Papisotiriou DG, Ibrahim M, Elkehal R, Karas M, Zickermann V, Gutensohn M *et al.* (2011) A high-definition native polyacrylamide gel electrophoresis system for the analysis of membrane complexes. *Plant J* **67**, 181–194.
- 33 Chan KM, Delfert D and Junger KD (1986) A direct colorimetric assay for Ca²⁺-stimulated ATPase activity. *Anal Biochem* **157**, 375–380.
- 34 Maehama T, Taylor GS, Slama JT and Dixon JE (2000) A sensitive assay for phosphoinositide phosphatases. *Anal Biochem* **279**, 248–250.
- 35 Rowlands MG, Newbatt YM, Prodromou C, Pearl LH, Workman P and Aherne W (2004) High-throughput screening assay for inhibitors of heat-shock protein 90 ATPase activity. *Anal Biochem* **327**, 176–183.
- 36 Gledhill JR, Montgomery MG, Leslie AGW and Walker JE (2007) Mechanism of inhibition of bovine F₁-ATPase by resveratrol and related polyphenols. *Proc Natl Acad Sci USA* **104**, 13632–13637.
- 37 Garcia-Amoros J, Sanchez-Ferrer A, Massad WA, Nonell S and Velasco D (2010) Kinetic study of the fast thermal *cis*-to-*trans* isomerisation of para-, ortho- and polyhydroxyazobenzenes. *Phys Chem Chem Phys* **12**, 13238–13242.
- 38 Kojima M, Nebashi S, Ogawa K and Kurita N (2005) Effect of solvent on *cis*-to-*trans* isomerization of 4-hydroxyazobenzene aggregated through intermolecular hydrogen bonds. *J Phys Org Chem* **18**, 994–1000.
- 39 Symersky J, Osowski D, Walters DE and Mueller DM (2012) Oligomycin frames a common drug-binding site in the ATP synthase. *Proc Natl Acad Sci USA* **109**, 13961–13965.
- 40 Yang I, Kim E, Kang J, Han H, Sul S, Park SB and Kim SK (2012) Photochemical generation of a new, highly fluorescent compound from non-fluorescent resveratrol. *Chem Commun* **48**, 3839–3841.
- 41 Maestro Schrödinger Release 2016-3: Maestro, Schrödinger (2016) LLC, New York, NY.
- 42 The PyMOL Molecular Graphics System, Version 1.2r1 Schrödinger. LLC, Mannheim, Germany.
- 43 Ahmad Z, Ahmad M, Okafor F, Jones J, Abunameth A, Cheniya RP and Kady IO (2012) Effect of structural modulation of polyphenolic compounds on the inhibition of *Escherichia coli* ATP synthase. *Int J Biol Macromol* **50**, 476–486.
- 44 Hoersch D (2016) Engineering a light-controlled F₁ ATPase using structure-based protein design. *PeerJ* **4**, e2286.
- 45 MacCarrone M, Lorenzon T, Guerrieri P and Agro AF (1999) Resveratrol prevents apoptosis in K562 cells by

- inhibiting lipoxygenase and cyclooxygenase activity. *Eur J Biochem* **265**, 27–34.
- 46 Park SJ, Ahmad F, Philp A, Baar K, Williams T, Luo H, Ke H, Rehmann H, Taussig R, Brown AL *et al.* (2012) Resveratrol ameliorates aging-related metabolic phenotypes by inhibiting cAMP phosphodiesterases. *Cell* **148**, 421–433.
- 47 Gehm BD, McAndrews JM, Chien PY and Jameson JL (1997) Resveratrol, a polyphenolic compound found in grapes and wine, is an agonist for the estrogen receptor. *Proc Natl Acad Sci USA* **94**, 14138–14143.

Supporting information

Additional Supporting Information may be found online in the supporting information tab for this article:

Fig. S1. UV irradiation experiment setup.

Fig. S2. Resveratrol binding site in the ATP synthase F₁ complex.

Fig. S3. ¹H NMR spectrum of PIAS-4.

Fig. S4. ¹³C NMR spectrum of PIAS-4.

Table S1. Reversible optical control of ATPase *in vitro* using purified *Y. lipolytica* ATP synthase.